



Measurement of spin-dependent total cross-section difference $\Delta\sigma_T$ in neutron-proton scattering at 16 MeV

**J. Brož, J. Černý, Z. Doležal¹, G.M. Gurevich², M. Jirásek,
P. Kubík, A.A. Lukhanin³, J. Švejda and I. Wilhelm**

Nuclear Centre, Charles University, V Holešovičkách 2, PRAGUE 8,
CZ-180 00 Czech Republic

**N.S. Borisov, Yu.M. Kazarinov, B.A. Khachaturov, E.S. Kuzmin,
V.N. Matafonov, A.B. Neganov, I.L. Pisarev, Yu.A. Plis and
Yu.A. Usov**

Joint Institute for Nuclear Research, Laboratory of Nuclear Problems, DUBNA,
Moscow Region, 141980 Russia

M. Rotter and B. Sedlák

Department of Low Temperature Physics, Faculty of Mathematics and Physics,
Charles University, V Holešovičkách 2, PRAGUE 8, CZ-180 00 Czech Republic

11 July 1995

¹electronic mail address dolezal@hp01.troja.mff.cuni.cz, fax +42-2-8576-2434

²on leave of absence from Institute for Nuclear Research, Russian Academy of Sciences, 60th
October anniversary prospect 7A, MOSCOW, 117312 Russia

³on leave of absence from Kharkov Institute of Physics and Technology, Academy Str. 1,
KHARKOV, 310108 Ukraine

Abstract

A new measurement of $\Delta\sigma_T$ for polarized neutrons transmitted through a polarized proton target at 16.2 MeV has been made. A polarized neutron beam was obtained from the ${}^3\text{H}(\text{d}, \bar{n}){}^4\text{He}$ reaction; proton polarization over 90% was achieved in a frozen spin target of 20 cm³ volume. The measurement yielded the value $\Delta\sigma_T = (-126 \pm 21 \pm 14)$ mb. The result of a simple phase shift analysis for the ${}^3S_1 - {}^3D_1$ mixing parameter ϵ_1 is presented and compared with the theoretical potential model predictions.

PACS numbers: 25.40.Dn, 24.70.+s, 13.75.Cs

Submitted to Zeitschrift für Physik A

1 Introduction

For the description of nucleon-nucleon (NN) forces semiphenomenological potential models are used [1, 2, 3]. However there are some discrepancies between various parametrizations, particularly in the isosinglet $n - p$ system. For the critical evaluation of potential models measurements of many variables in a wide range of energies are necessary. From the existing reviews (e.g. [4]) of NN scattering experiments one can see that there are numerous measurements of pp scattering (contributing to the description of $I = 1$ system), but only sparse data exists for the $n - p$ system. This situation is even worse at low energies (below 100 MeV), especially for polarized experiments. However the importance of spin-dependent observables for the nuclear interaction theory development is evident.

Optical theorem shows that cross-sections (unlike other observables) depend linearly on the scattering amplitudes so they give us a more direct information for the understanding of the NN forces. The lack of data in the low energy region is visible from the Fig. 1, where the situation in the measurement of np spin-dependent total cross-section difference for beam and target spin orientation transverse to the beam direction $\Delta\sigma_T$ below 1200 MeV is plotted together with the phase-shift solution SP95 from SAID [5, 6].

Besides their general importance for the phase-shift analysis (PSA) $\Delta\sigma_T$ values at the energies below 100 MeV have showed their high sensitivity to the ${}^3S_1 - {}^3D_1$ mixing parameter ϵ_1 which is considered to be ill-determined by several authors [7]. This mixing parameter measures the strength of a tensor component of the NN forces and can be determined from only a few other observables which have a high contribution of the coupled triplet. Taking into account the formulae for the observables deduced in [8] together with experimental possibilities one comes to the spin correlation coefficient $A_{yy}(\vartheta)$ (or A_{00nn} in the Saclay four-subscript notation [8]) at 90° c.m. angle (at this angle some amplitudes cancel due to their antisymmetric behaviour) and the spin transfer parameter $K_y^{y'}(\vartheta)$ (or K_{0nn0}). Analysis of their measurements shows apparent discrepancies from the potential model predictions (see subsect. 4.3).

In this paper results from a new measurement of $\Delta\sigma_T$ in neutron-proton scattering at 16.2 MeV are presented.

2 Experimental setup

The measurement of $\Delta\sigma_T$ has been performed using the classical transmission method, i.e. the relative difference in attenuation of a polarized neutron beam passing a polarized proton target was measured.

2.1 Polarized proton target

In the present experiment the frozen spin polarized proton target has been used. The target is a complex device consisting of several blocks:

- High power $^3\text{He}/^4\text{He}$ dilution refrigerator
- Movable magnetic system providing a "warm" field and consisting of a superconducting solenoid and a superconducting dipole holding magnet with a large aperture
- Electronic equipment for providing proton polarization and measurement of its value.

1,2-propanediol with a paramagnetic Cr(V) impurity was used as a target material. Beads of this material approximately 2 mm diameter were cooled to liquid nitrogen temperature and placed inside a perforated teflon ampule 2 cm in diameter and 6 cm length. The ampule was then loaded into a horizontal mixing chamber of the dilution refrigerator using a lock device. A horizontal part of the refrigerator containing almost 20 cm³ of propanediol with a total mass of about 15 g was placed in a neutron beamline.

The hydrogen nuclei in the propanediol were polarized by a dynamic nuclear orientation technique at a temperature 0.3-0.4 K in a strong highly uniform magnetic field (2.7 T) using 75 GHz hyperfrequency. This magnetic field within the target volume was produced by the superconducting solenoid in the dynamic polarization regime. Maximum values of the proton polarization obtained were 93% and 98% for positive and negative polarizations, respectively. The time needed to achieve 80% of maximum polarization is about one hour. The target polarization value was calculated by comparison of the amplified polarized proton NMR signal with a thermal equilibrium NMR signal measured at about 1 K temperature in the same magnetic field. The accuracy of the polarization determination was approximately $\pm 3\%$. This uncertainty is due to the evaluation of integrated thermal equilibrium signal and to the measurement of temperature.

After achieving a high proton polarization the solenoid field is decreased while the holding magnet field is increased. Finally, the solenoid is removed from the vicinity of the target leaving it in 0.37 T vertical magnetic field produced by the holding magnet. The latter provides $\pm 50^\circ$ aperture in the vertical plane and nearly 360° aperture in the horizontal plane. The final temperature of the target in the frozen mode is around 20 mK. The spin relaxation time for protons measured in these conditions was approximately 1000 hours for positive polarization and 300 hours for negative polarization. As a result, a polarization degradation during one continuous experimental run of 10-12 hours was always insignificant.

A more detailed description of the target complex is given in [9].

2.2 Polarized neutron beam

The polarized neutron beam is produced as a secondary beam via the ${}^3\text{H}(d, n){}^4\text{He}$ reaction. An unpolarized deuteron beam with $E_d = 1.825$ MeV from the Van de Graaff electrostatic accelerator HV 2500 AN strikes a Ti-T target (2 mg/cm^2) on a molybdenum backing at an angle of 45° . To achieve a monoenergetic collimated neutron beam, the associated particle method is used. The principle of the method is as follows: knowing the incident projectile energy in two-body reaction (using a thin target), the energy and angle of emitted particle and recoil nucleus are kinematically conjugated. In our case a collimated beam of recoil alpha particles registered in the charged particle detector at a definite angle is associated with neutrons of known energy and average angle emitted in a narrow cone. The experimental setup is shown in Fig. 2. For incident deuteron energies comparable to the recoil alpha-particle energy, the charged particle detector suffers from elastically scattered deuterons whose intensity relative to the number of alpha-particles is higher by several orders of magnitude (due to the high Coulomb cross-section). To avoid this background we deflected parasitic deuterons from the alpha-particles using a magnetic separator. Hence the recoil alpha-particles emitted at the laboratory angle of 90° to the primary deuteron beam together with the deuterons elastically scattered at the same angle passed through the perpendicular magnetic field of 0.5 T. The silicon surface-barrier (SSB) detector ($8 \times 5 \text{ mm}^2$) was adjusted to the position corresponding to alpha-particles curvature in the separator magnetic field, so it detected only a small part of the original deuteron flux. Neutrons associated with the alpha-particles, which registered in the SSB detector, were emitted to the narrow cone (FWHM = 18 mm at 1 m distance from the tritium target), which corresponds to the aperture diameter in the shielding block ($0.6 \times 1.4 \times 1.4 \text{ m}^3$).

In the experiment described here the associated neutron beam with an energy $E_n = (16.2 \pm 0.1)$ MeV was emitted at an angle $\vartheta_{lab} = (62.0 \pm 0.7)^\circ$. In spite of using the unpolarized incident deuteron beam the outgoing neutron beam is partially polarized. Its polarization in this energy region has been measured several times [10, 11], but the recent measurement in Tübingen [12] covers a large range of energies and angles with minimal error. Interpolating these results we have obtained $P_b = (-13.5 \pm 1.4)\%$ (see 4.2)

The neutron production and detection system has been described in a detail in [13].

2.3 Neutron detection system

The neutron beam incident on the polarized proton target is monitored by two plastic scintillator detectors viewed via a 60 cm long light guide (to eliminate the magnetic field effects) by fast photomultipliers (PM) XP 2020 (monitor MON1: $3 \times 20 \times 20 \text{ mm}^3$, monitor MON2: $10 \times 30 \times 30 \text{ mm}^3$).

Two liquid scintillator (NE-213) detectors DET1 and DET2 of cylindrical shape (\varnothing 40 mm \times 60 mm) were placed behind the polarized proton target. These detectors were also mounted to XP 2020 PM's. All the detectors were located in the neutron beam axis. A schematic diagram of the electronic circuit is shown in Fig. 3. The preamplifier attached to the semiconductor detector gives two outputs: fast timing signals and slow amplitude (proportional to energy) signals.

The slow (energy) signal is amplified, fed into a linear gate and stretcher, and then passed to the analog-to-digital converter ADC1. The fast signal is shaped in a constant-fraction discriminator (CFD) and fed along with the signals from the neutron detectors, also shaped in CFD's, to the coincidence control unit. This specially constructed programmable coincidence control unit with resolving time equal to 100 ns allows registration of any combination of 8 input signals defined by the control software while the registration of any undefined combination is disabled. For our experiment the coincidences of signals from one alpha and any (but only one) neutron detector (out of four) were enabled, any coincidences between neutron detectors (coming from the multiple neutron scattering from one detector to another or from the background) were disabled. The output digital signal from this unit gives information about the type of coincidence, i.e. in our case the serial number of the neutron detector in coincidence with the alpha-particle detector.

Another output signal from the alpha-particle CFD is fed to the time-to-amplitude converter (TAC) as a START signal. STOP signal is derived from the fast summator fed with CFD's signals corresponding to the neutron detectors (this solution enables us to use only one TAC). In order to minimize the dead time of the TAC it is gated by a fast coincidence signal (formed from the same signals as TAC) with resolving time equal to full scale of TAC (100 ns) with a short delay time of response (maximally 110 ns after the START signal). The output signal from TAC is fed to ADC2. Both the ADC's are gated by the output signal of the coincidence control. Information from these two ADC's along with the coincidence type number from the coincidence control unit is fed to the computer via the CAMAC crate controller and parallel computer interface.

3 Experimental procedure

3.1 Formalism

The expression for the nucleon-nucleon total cross-section for polarized beam and target (deduced in [14] and [15] and discussed in [8]) can be written as

$$\sigma_{tot} = \sigma_{0,tot} + \sigma_{1,tot}(\vec{P}_b\vec{P}_t) + \sigma_{2,tot}(\vec{P}_b\vec{k})(\vec{P}_t\vec{k}) \quad (1)$$

where \vec{P}_b and \vec{P}_t are the polarization vectors of the beam and the target, respectively, and \vec{k} is a unit vector in the beam direction. For transverse and

longitudinal spin directions and complete polarizations

$$|\vec{P}_b| = |\vec{P}_t| = 1 \quad (2)$$

we define the observables $\Delta\sigma_T$ and $\Delta\sigma_L$ as

$$\Delta\sigma_T = \sigma(\uparrow\downarrow) - \sigma(\downarrow\downarrow) = -2\sigma_{1,tot} \quad (3)$$

$$\Delta\sigma_L = \sigma(\rightleftharpoons) - \sigma(\rightarrow) = -2(\sigma_{1,tot} + \sigma_{2,tot}) \quad (4)$$

The relative difference in attenuation of a polarized neutron beam after passing through the polarized proton target for parallel and antiparallel spin orientations is

$$\xi(c) = \frac{N_d(c)}{N_{mon}(c)} \quad (5)$$

where N_d and N_{mon} are net areas under the time-of-flight peak in the measured spectra from detector and monitor, respectively, and c denotes the spin orientation combination ($c = \uparrow\downarrow$ or $\downarrow\downarrow$).

Assuming that the detector efficiencies η_d and η_{mon} are constant for all measurements (see subsect. 4.2) and the degrees of beam and target polarizations are P_b and P_t , respectively, we have

$$N_d(\uparrow\downarrow) = \eta_d I_0(\uparrow\downarrow) \exp[-\omega\sigma(\uparrow\downarrow)] = \eta_d I_0(\uparrow\downarrow) \exp[-\omega(\sigma_0 + \frac{1}{2}\Delta\sigma_T P_b P_t)] \quad (6)$$

$$N_d(\downarrow\downarrow) = \eta_d I_0(\downarrow\downarrow) \exp[-\omega\sigma(\downarrow\downarrow)] = \eta_d I_0(\downarrow\downarrow) \exp[-\omega(\sigma_0 - \frac{1}{2}\Delta\sigma_T P_b P_t)] \quad (7)$$

$$N_{mon}(c) = \eta_{mon} I_0(c) \quad (8)$$

where ω is the number of protons per unit area of the target and $I_0(c)$ is the integrated beam intensity.

Hence for $\Delta\sigma_T$ we finally have

$$\Delta\sigma_T = \frac{\ln(\xi(\downarrow\downarrow)) - \ln(\xi(\uparrow\downarrow))}{\omega P_b P_t} \quad (9)$$

3.2 Data collection

The measurement was divided into 14 runs. During each run the target polarization remained unchanged. Before the run the proton target polarization was built up and measured. Data consisting of ADC1 channel, ADC2 channel and the serial number of the neutron detector were buffered and recorded on tape in 100-event-blocks together with other important information (total counts in energy and time channel from the alpha detector as well as from the individual

neutron detectors, total time elapsed, etc.) During the data acquisition some results were available from the on-line monitoring program.

Immediately after each run the target polarization was measured and either reversed or restored in its original magnitude for the next run.

The total data taking time was 91 hours for antiparallel and 85 hours for parallel orientation of spins. During this time 8×10^6 antiparallel and 7×10^6 parallel net $n - \alpha$ coincidences were recorded to tape. The typical gross coincidence count rate was 50 s^{-1} for approximately 10^4 s^{-1} count rates in both alpha and neutron channels. The deuteron beam current on Ti-T target was kept below $5 \mu\text{A}$.

4 Results and discussion

4.1 $\Delta\sigma_T$ determination

In the course of data reduction 2-parameter histograms (ADC1 vs. ADC2) for each neutron detector were created from tapes (see Fig. 4). A window in the energy spectrum was set to eliminate elastically scattered deuterons (see 2.3). Fig. 5 shows the typical charged particle energy spectrum and Fig. 6 shows the neutron time-of-flight spectrum. Time resolution achieved in this experimental setup with a residual magnetic field from the polarized proton target was about 3 ns, the resolution with the magnets off can be reduced down to 1.5 ns. Applying this cut also reduced background of random coincidences in the time-of-flight spectrum by a factor of roughly 2. The remaining accidental background was linear in a wide range of channels on both sides of the peak, so that a linear approximation and subtraction could be used to calculate the net peak area. The resulting area appeared to be fairly independent of the variation of left and right peak borders. Then four ratios of net areas from two detectors and two monitors were calculated for each 10^5 events. The stability control was enabled by two additional ratios MON2:MON1 and DET2:DET1.

For both target spin orientations the weighted centroids of all runs were calculated

$$\langle \xi \rangle = \frac{\sum \frac{\xi_i P_i}{\sigma_i^2}}{\sum \frac{P_i}{\sigma_i^2}} \quad (10)$$

$$\langle P_t \rangle = \frac{\sum \frac{P_i}{\sigma_i^2}}{\sum \frac{1}{\sigma_i^2}} \quad (11)$$

These centroid values of the target polarization P_t and the resulting ratio ξ were then used to calculate the spin-dependent total cross-section difference $\Delta\sigma_T$ from Eq. 9. The final values were obtained as a weighted mean of the four relevant ratios.

From our measurement we have obtained the result

$$\Delta\sigma_T = (-126 \pm 21 \pm 14) \text{ mb} \quad (12)$$

where the first uncertainty is the statistical error and the second uncertainty is due to systematic errors (see subsect. 4.2). Comparison of our measured value with theoretical predictions as well as with TUNL measurements is plotted in Fig. 7.

4.2 Systematic errors and instrumental asymmetries

To estimate the final uncertainty of $\Delta\sigma_T$ originating from systematic effects several sources of errors were analysed. They can be divided into two groups: polarization-dependent effects which introduce a false asymmetry, and polarization-independent effects included in the systematic error.

When evaluating polarization-dependent effects we did not restrict ourselves only to the effects directly connected to the spins, but we studied also side effects of polarization: magnetic fields orientation, beam position, etc.

The use of the polarized proton target with identical holding magnetic fields for both spin orientations is a great advantage for this kind of measurement. To ensure this we measured the magnetic field intensity during the data collection near the photomultiplier tubes. The monitoring showed that the relative changes from one polarization to another as well as those during the run were less than $3 \cdot 10^{-3}$, and as negligibly small were not taken into account.

The displacement of neutron detectors can be another possible source of false asymmetries. Due to a non-zero analyzing power A_y as well as the spin correlation coefficients A_{yy} and A_{xx} , the left-right and up-down asymmetry for small angle np elastic scattering cross-section exists. When the detectors are placed symmetrically with respect to the beam line the differences will be averaged out, but any displacement will cause a non-zero contribution to the measured spin-dependent cross-section. Our calculations show that the maximal relative contribution does not exceed $4 \cdot 10^{-3} \text{deg}^{-1} \approx 10^{-4} \text{mm}^{-1}$. The tolerance of the detector adjustment is below 2 mm, so this source of false asymmetry can be neglected.

Systematic error consists of several polarization-independent effects: errors in determining the beam and target polarizations, error in target density, polarization-independent effects of beam and detector geometry and variation of detector efficiencies (due to instabilities of high voltage, gains, thresholds, etc.).

The uncertainty of the neutron beam polarization manifests itself as a major source of the final error. We have taken the experimental values of polarization obtained in 1991 in Tübingen [12], because they cover both the energy and the angular region of our interest. The measured values were fitted (using 2nd order polynomial for energy dependence and Legendre polynomials for the angular dependence) and the resulting value for $E_d = 1.825 \text{ MeV}$ and $\vartheta = 62^\circ$ was taken.

Because $\chi^2/N_{d.o.f.} = 1.2$ and our angle is close to the measured angles 50° and 70° , we kept the original absolute error 1.4 % which represents 10 % relative error of P_b and has a scale character.

The target polarization was measured with 3% relative error (see subsect. 2.1). The density of the target was determined by precision weighing with 3% relative error.

Geometrical displacement of detectors, beside its contribution to the false asymmetry represents also a source of systematic error due to the beam divergence and finite solid angle of the detectors. Since detectors were not removed during the whole measuring period, this contribution was equal for both target spin orientations and this error is a scale error. Calculations based on the beam profile show relative contribution of 0.8% for 2 mm displacement (equal to the tolerance of detector adjustment). The uncertainty originating from the beam position variations (≈ 1 mm) is about 0.1%.

Use of scintillators attached to the photomultipliers represents a considerable source of uncertainties (PM's are very sensitive to the instability of high voltage applied, the thresholds and gains of electronic modules used can float, etc.). It should be noted that each PM was fed from an independent high voltage supply. We have performed a set of tests including the long-time monitoring of high voltage supplies stability (within ± 1 V at 2000 V), runs with a “dummy” target without magnetic fields as well as the analysis for two additional ratios MON2:MON1 and DET2:DET1 (see subsect. 4.1). All these tests yielded values consistent with zero within error bars of 15 mb.

4.3 The mixing parameter ϵ_1

Before we start the discussion on the influence of our measured value to the determination of the mixing parameter ϵ_1 , we describe briefly the experimental situation in the measurement of ϵ_1 -related observables. The $A_{yy}(\vartheta)$ measurement at 90° c.m. is presented by Schöberl et al. [16] for 13.7 MeV neutron energy (Erlangen) and by Doll et al. [17] for 19, 21 and 25 MeV (Karlsruhe). The spin transfer parameter $K_y^{y'}(133^\circ_{c.m.})$ was measured at 25.8 and 17.4 MeV by Ockenfels et al. [18, 19] (Bonn), while $\Delta\sigma_T$ was only recently measured in TUNL in the 3.65-11.60 MeV energy range [20, 21]. In all these works the authors performed at least basic phase shift analyses to determine the value of ϵ_1 , in order to compare the experimental results from different experiments. From the analyses (see Table 1 reprinted from [20]) it is evident that relative agreement exists between individual experiments and potential model predictions, but there are some indications of discrepancies between 13 and 20 MeV towards weaker tensor force. These indications were also supported by results published from TUNL [20] for $E_n=7.43$, 9.57 and 11.6 MeV. In the meantime, the authors announced corrected values (by about 20%) [21] where the discrepancies are not so apparent. However there are experimental results supporting the hypothesis of lower tensor force around 15

MeV. This is in contradiction to the result obtained by the Basel group with an experiment performed at Villigen [22, 23], where $\Delta\sigma_L$ has been measured at 66 MeV incident neutron energy and the analysis made by Henneck [24]. In these works the authors conclude that the tensor component of NN potential below 100 MeV must be stronger than predicted by the models.

As seen from Fig. 7 our new value of $\Delta\sigma_T$ is in general agreement with potential model predictions as well as with the TUNL measurements. The comparison of other direct experimental results in the field (see Introduction) is impossible so a phase-shift analysis must be performed and resulting ϵ_1 mixing parameter values compared. Since it is not easy to perform a complete PSA, most of the authors restrict themselves to varying only few (or even one) phase parameter, while fixing the others at the values from certain potential model or PSA, with a risk of introducing ambiguities in the comparisons. In the most extensive analysis of ϵ_1 -oriented experiments below 30 MeV presented by Wilburn [20], only ϵ_1 was varied, while the remaining phase parameters were taken from the Bonn B potential. We evaluated the sensitivity of $\Delta\sigma_T$ to different phase shifts and mixing parameters (using the full Bonn potential set), and the resulting contributions (see Table 2) justify the single parameter analysis to be performed here.

The spin-dependent total cross-section difference $\Delta\sigma_T(np)$ can be written as

$$\Delta\sigma_T(np) = \frac{1}{2}(\Delta\sigma_T(I = 0) + \Delta\sigma_T(I = 1)) \quad (13)$$

where I is the isospin, or in terms of the phase-shifts in the Stapp convention [25, 26]

$$\Delta\sigma_T = \frac{\pi}{k^2} \left\{ \begin{array}{l} [3 \cos 2\delta_{1P_1} - \cos 2\delta_{3S_1} - 2 \cos 2\delta_{3D_1} \\ + 2\sqrt{2} \sin(\delta_{3D_1} + \delta_{3S_1}) \sin 2\epsilon_1 + \dots] \\ + [\cos 2\delta_{1S_0} - \cos 2\delta_{3P_0} \\ + 5 \cos 2\delta_{1D_2} - 2 \cos 2\delta_{3P_2} - 3 \cos 2\delta_{3F_2} \\ + 2\sqrt{6} \sin(\delta_{3P_2} + \delta_{3F_2}) \sin 2\epsilon_2 + \dots] \end{array} \right\} \quad (14)$$

where δ_i is the phase-shift of a state i (in a spectroscopic notation), ϵ_J is the mixing parameter of states with total angular momentum J , and k is a neutron impulse in the centre-of-mass system. One can see from these expressions that when the experimental difficulties are overcome and the spin-dependent cross-section for pp elastic scattering is measured at this energy, $\Delta\sigma_T(I = 1)$ will be known and the number of phase parameters to be varied will be reduced considerably.

For our value of $\Delta\sigma_T$ the resulting mixing parameter is

$$\epsilon_1 = (1.5 \pm 1.3)^\circ \quad (15)$$

The present situation in this energy region is displayed in Fig. 8, where the results from Table 1 are plotted together with our new result and with model predictions.

5 Conclusion

A measurement of the spin-dependent total cross-section difference $\Delta\sigma_T$ for the scattering of polarized neutrons from polarized protons at 16 MeV has been made with the resulting value

$$\Delta\sigma_T = (-126 \pm 21 \pm 14) \text{ mb} \quad (16)$$

All effects possibly influencing the accuracy of the result have been critically evaluated and the quoted uncertainty safely encompasses all these effects.

A phase-shift analysis has been performed, varying the mixing parameter ϵ_1 while the other phase parameters were kept constant and equal to the full Bonn potential model predictions. This PSA gave the result

$$\epsilon_1 = (1.5 \pm 1.3)^\circ \quad (17)$$

From this result one can conclude that the presented values do not support the hypothesis of local minimum of ϵ_1 around 15 MeV, representing a much weaker tensor force than that predicted (as indicated in [16, 19, 20]).

Since the degree of our neutron beam polarization is rather low, the error of its determination dominates the final error. Any reduction of the uncertainty of $\Delta\sigma_T$ using our current setup seems unfeasible.

One promising way to obtain more precise experimental data for the phase-shift analysis using the setup described here is to combine more observables. Tornow et al. [27] have shown that the combination of the spin-dependent total cross-section differences for transverse and longitudinal polarizations $\Delta\sigma_T$ and $\Delta\sigma_L$ can reduce the resulting inaccuracy in ϵ_1 determinations. As far as we are informed the $\Delta\sigma_L$ measurement is to be performed in TUNL [28]. Our experimental apparatus will be modified to allow both beam and target spins to be oriented in the longitudinal direction. We are preparing the $\Delta\sigma_L$ measurement, as we believe that new measurements are needed to clarify the tensor contribution to the NN potential in the low energy region.

6 Acknowledgment

The authors express their gratitude to J. Formánek, N.A. Russakovich and I. Úlehla for their valuable contribution to the physics program of this experiment and support and to F. Lehar for careful reading of the manuscript and helpful comments. Furthermore we thank M. Navrátilová, V.G. Kolomiets and O.N. Shchevelev for their assistance in carrying out the experiments. The authors gratefully acknowledge the financial support from the Grant Agency of Czech Republic under the registration No. 202/93/2426 for whom the work was performed.

References

- [1] Lacombe M. , Loisseau B., Richard J.M., Vinh Mau R., Coté J., Pirès P. and de Tourreil R., Phys. Rev. C **21**(1980)861
- [2] Machleidt R., Holinde K. and Elster C., Phys.Rep. **149**(1987)1
- [3] Stoks V.G.J., Klomp R.A.M., Terheggen C.P.F. , de Swart J.J, Phys. Rev. C **49**(1994)2950
- [4] Lechanoine-LeLuc C., Lehar F., Rev. Mod. Phys. **65**(1993) 47-86.
- [5] Arndt R.A., Strakovsky I.I. and Workman R.L., Phys. Rev. C **50**(1994)1796
Arndt R.A., Strakovsky I.I. and Workman R.L., Phys. Rev. C **50**(1994)2731
- [6] Arndt R.A., Strakovsky I.I., phase-shift solutions VZ40,SM95, 1995 (private communication)
- [7] Binstock J. and Bryan R., Phys. Rev. D **9**(1974)2528
- [8] Bystricky J., Lehar F. and Winternitz P., J.Phys. (Paris) **39**(1978)1
- [9] Borisov N.S., Matafonov V.N., Neganov A.B., Plis Yu.A., Schevelev O.N., Usov Yu.A., Jánský I., Rotter M., Sedlák B., Wilhelm I., Gurevich G.M., Lukhanin A.A., Jelínek J., Srnka A. and Skrbek L., Nucl.Instr.&Meth. A **345**(1994)421
- [10] Levintov I.I., J.Exp.Theor.Phys. **34**(1958)1030
- [11] Perkins R.B., Simmons J.E., Phys. Rev. **124**(1961)1153
- [12] Koch M., Kolatschek J., Bürkle W., Mertens G., Lukas D., Müller H.M. and Langange K., talk at the Nucl.Phys. Spring Meeting, Salzburg, 1992
Kolatschek J., private communication 1992
- [13] Wilhelm I., Murali P. and Doležal Z., Nucl.Instr.&Meth. A **317**(1992)553
- [14] Bilenky, S.M. and Ryndin, R.M., Phys.Lett. **6**(1963)217
- [15] Phillips R.J.N., Nucl.Phys. **43**(1963)413
- [16] Schöberl M., Kuiper H., Schmelzer R. and Tornow W., Nucl.Phys. A **489**(1988)284
- [17] Doll P., Eberhard V., Fink G., Finlay W., Ford T.D., Heeringa W., Klages H.O., Krupp H. and Wölfl,Ch., in Contributed Papers to the XIIth Int.Conf.on Few-Body Problems in Physics, Vancouver 1989, in Few Body XII, ed. by B.K. Jennings, TRIUMF Report No. TRI-89-2,C16

- [18] Ockenfels M., Meyer F., Köble T., von Witsch W., Weltz J., Wingender K. and Wollman G., Nucl. Phys. A **526**(1991)109
- [19] Ockenfels M., Köble T., Schwindt M., J. Weltz and W. von Witsch, Nucl. Phys. A **534**(1991)248
- [20] Wilburn W.S., Gould C.R., Haase D.G., Huffman P.R., Keith C.D., Koster J.E., Roberson N.R. and Tornow W., Phys. Rev. Lett. **71**(1993)1982
- [21] Tornow W., talk at the 8th Int. Conf. on Polarization Phenomena in Nuclear Physics, Bloomington 1994, to be published
- [22] Haffter P., Brogli-Gysin C., Campbell J., Frotschi D., Götz J., Hammans M., Henneck R., Jourdan J., Masson G., Qin L.M., Robinson s., Sick I., Tuccillo M., Konter J.A., Mango S. and van den Brandt B., Nucl. Phys. A **548**(1992)29
- [23] Sick I., Contributed Paper, in Few Body Systems, Suppl.6(1992)128
- [24] Henneck R., Phys. Rev. C **47**(1993)1859
- [25] Wilburn W.S., Ph.D. Thesis, Duke University, 1993
- [26] Tornow W., in Spin and Isospin in Nucl. Interactions, ed. by Wissinck S.W., Goodman C.D. and Walker G.E., Plenum Press, N.Y., 1991, p. 461
- [27] Tornow W., Baker O.K., Gould C.R., Haase D.G., Roberson N.R. and Wilburn W.S., Proc. Conf. Physics with Polarized Beams on Polarized Targets, Spencer 1989.
- [28] Tornow W., private communication 1994
- [29] Binz R., van den Brandt B., Buchle R., Daum M., Demierre P., Franz J., Gaillard G., Hamann N., Hess R., Konter J.A., Lehar F., Lechanoine-Leluc C., Mango S., Peschina R., Perrot-Kunne F., Rapin D., Rössle E., Schmelzbach P.A., Schmitt H., Todenhagen R., Nucl.Phys. A**533**(1991)601
- [30] Adams D., Arvieux J., Azaiez H., Bach P., Ball J., Barabash L.S., Binz R., Bystricky J., Chaumette P., Demierre P., Derégel J., Fontaine J.M., Gaillard G., Ghazikhanian V., Gordon J., Hasegawa T., Hess R., Janout Z., Khachaturov B.A., Klett A., Kunne R., Lac C.D., Lehar F., Lemaire M.C., de Lesquen A., Lopiano D., de Mali M., Michalowicz A., Newsom C.R., Onel Y., Penzo A., Perrot- Kunne F., Peschina-Klett R., Rapin D., Raymond C., Rössle E., van Rossum L., Schmitt H., Sans J.L., Sormani P., Spinka H., Usov Yu.A., Vuaridel B. and Whitten C.A., accepted for publication in Acta Polytechnica, Czech Technical University Prague

Figure captions

Fig.1 $\Delta\sigma_T$ measurements for the np elastic scattering below 1200 MeV with the phase-shift solution - vertical axis shows $\frac{x}{|x|}\sqrt{|x|}$, where $x = \Delta\sigma_T$ in mb (line - SM95 solution from SAID [5, 6], squares - TUNL [20, 21], circle - this work, up triangles - PSI [29], down triangles - Saturne II [30])

Fig.2 Top view of the experimental setup 1. Deuteron beam 2. Ti-T target 3. Alpha-particle beam 4. Magnetic separator 5. Silicon surface-barrier detector 6. Neutron beam monitor MON1 7. Collimator and shielding 8. Neutron beam monitor MON2 9. Neutron beam 10. Polarized proton target 11. Neutron detector DET1 12. Neutron detector DET2

Fig.3 Schematic diagram of the electronic circuit (for further description see subsect. 2.2 and 2.3)

SSB: Silicon surface-barrier detector
PA: Preamplifier Canberra
SA: Spectroscopic amplifier Tennelec TC-244
S: Liquid scintillator NE-213
PMT: Photomultiplier tube Philips XP-2020
LG&S: Linear gate & stretcher Ortec 542
CFD: Constant fraction discriminator Tennelec TC-454
TAC: Time to amplitude converter Tennelec TC-816A
ADC: Analog to digital converter Tesla NL-2320
FC: Fast coincidence (Nuclear Centre)
CC: Coincidence control (Nuclear Centre)
SUM: Fast summator (Nuclear Centre)
MPU: Multiparameter unit (Nuclear Centre)
Variable delay Polon 1506
CAMAC crate controller Tesla NL-2106

Fig.4 Scatterplot of 2-parameter histogram: x-axis corresponds to the neutron detector time-of-flight (ADC2) spectrum, y-axis corresponds to the energy spectrum of the SSB detector (ADC1).

Fig.5 Energy spectrum of the SSB detector: solid line – original spectrum, hatched area – spectrum gated with $\alpha - n$ coincidences (the deuterons are well suppressed, see subsect. 2.2)

Fig.6 Time-of-flight spectrum from the neutron detector

Fig.7 Comparison of existing $\Delta\sigma_T$ measurements and potential model predictions (circles - TUNL [20, 21], triangle - this work, lines: solid - Bonn, dashed - Paris, dotted - Nijmegen)

Fig.8 Values of ϵ_1 analysed from available data (full squares - TUNL [20, 21], diamond - Erlangen [16], open square - this work, open triangles - Karlsruhe [17], full triangles - Bonn [18, 19], lines: solid - Bonn potential, dashed - Nijmegen, dotted - Paris, dashed-dotted - Low energy (0-400 MeV) solution VZ40 from SAID [5, 6])

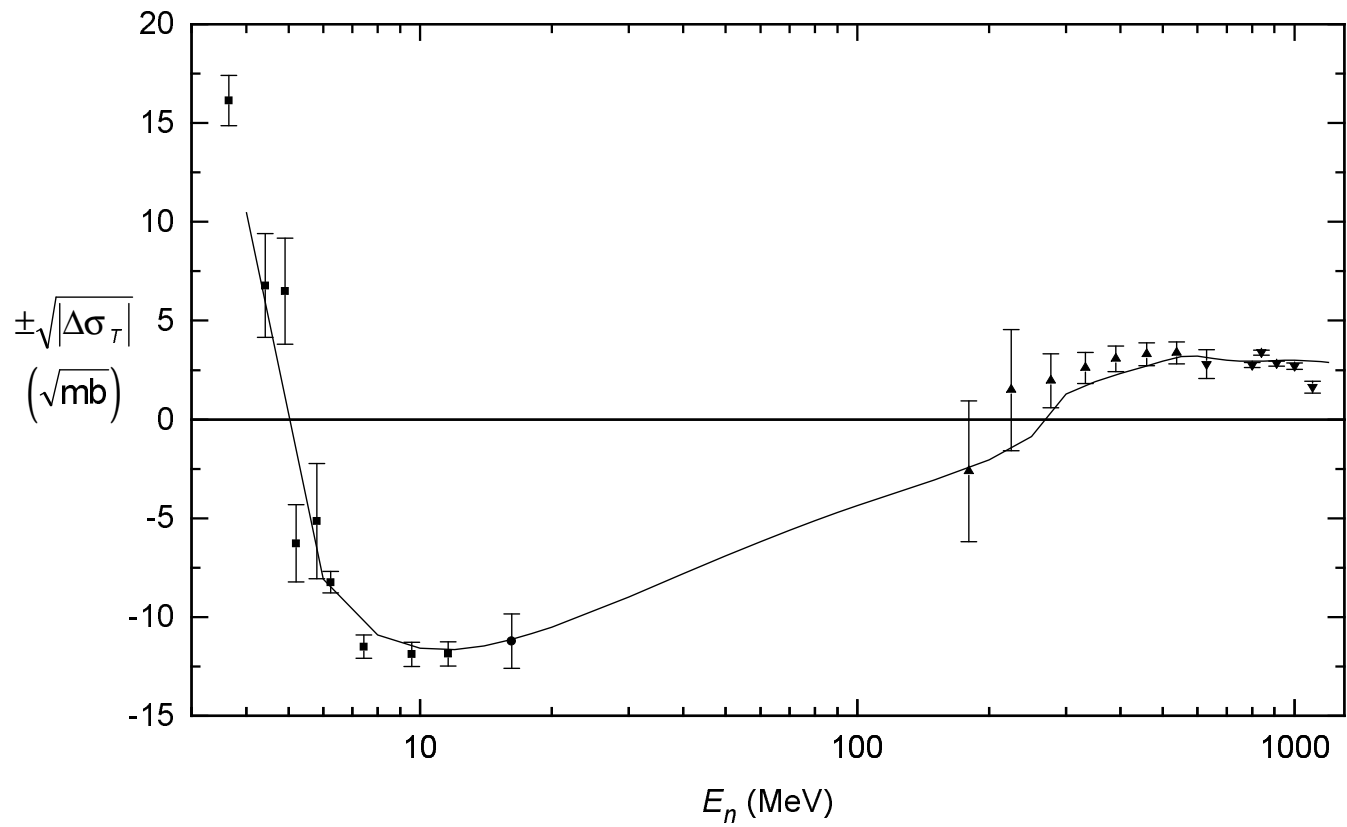
Table 1: Values of ${}^3D_1 - {}^3S_1$ mixing parameter ϵ_1 from presently available data

E_n (MeV)	ϵ_1 (degrees)	Observable	Ref.
5.1	0.41 ± 0.22	$\Delta\sigma_T$	[20, 21]
7.4	0.54 ± 0.43	$\Delta\sigma_T$	[20, 21]
9.6	1.32 ± 0.51	$\Delta\sigma_T$	[20, 21]
11.6	1.50 ± 0.64	$\Delta\sigma_T$	[20, 21]
13.7	-0.16 ± 0.50	A_{yy}	[16]
17.4	-0.94 ± 1.11	$K_y^{y'}$	[19]
19.0	1.20 ± 0.94	A_{yy}	[17]
22.0	1.46 ± 0.66	A_{yy}	[17]
25.0	2.64 ± 0.68	A_{yy}	[17]
25.8	2.60 ± 0.40	$K_y^{y'}$	[18]

Table 2: Sensitivity of $\Delta\sigma_T$ to changes in phase-shifts and mixing parameters in relative units (for the full Bonn set)

δ_{1S_0}	δ_{3P_0}	δ_{1P_1}	δ_{3P_1}	δ_{3S_1}	ϵ_1	δ_{3D_1}	δ_{1D_2}	δ_{3D_2}	δ_{3P_2}	δ_{3F_2}	ϵ_2
0.19	0.05	0.11	0.00	0.01	0.57	0.02	0.01	0.00	0.01	0.01	0.03

Figure 1



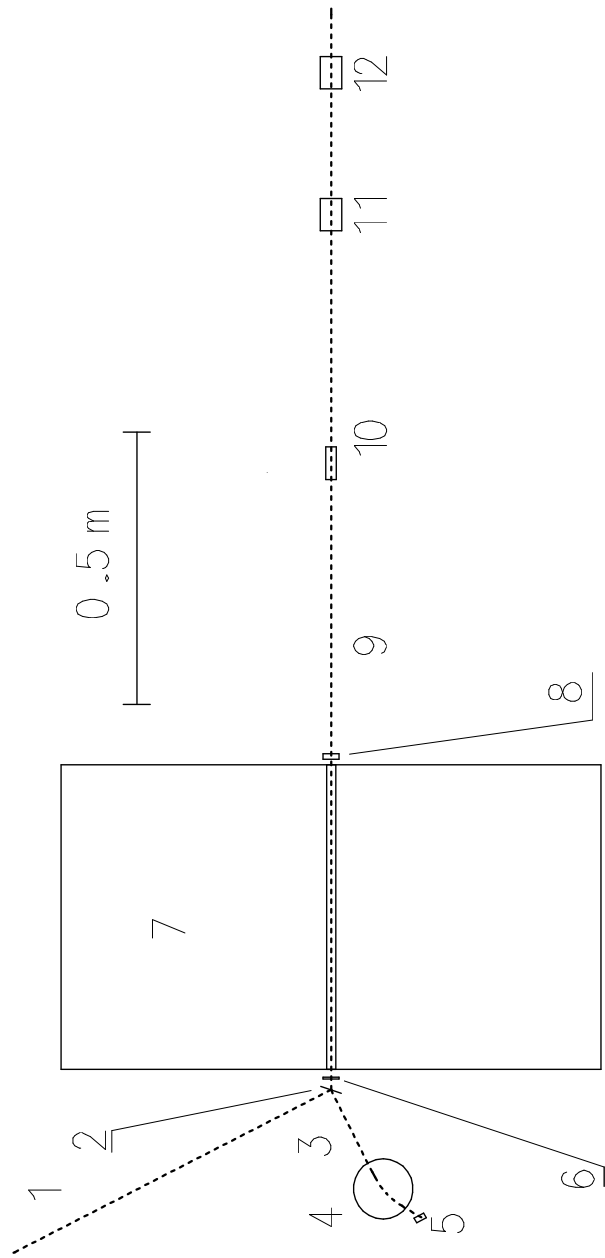


Figure 2

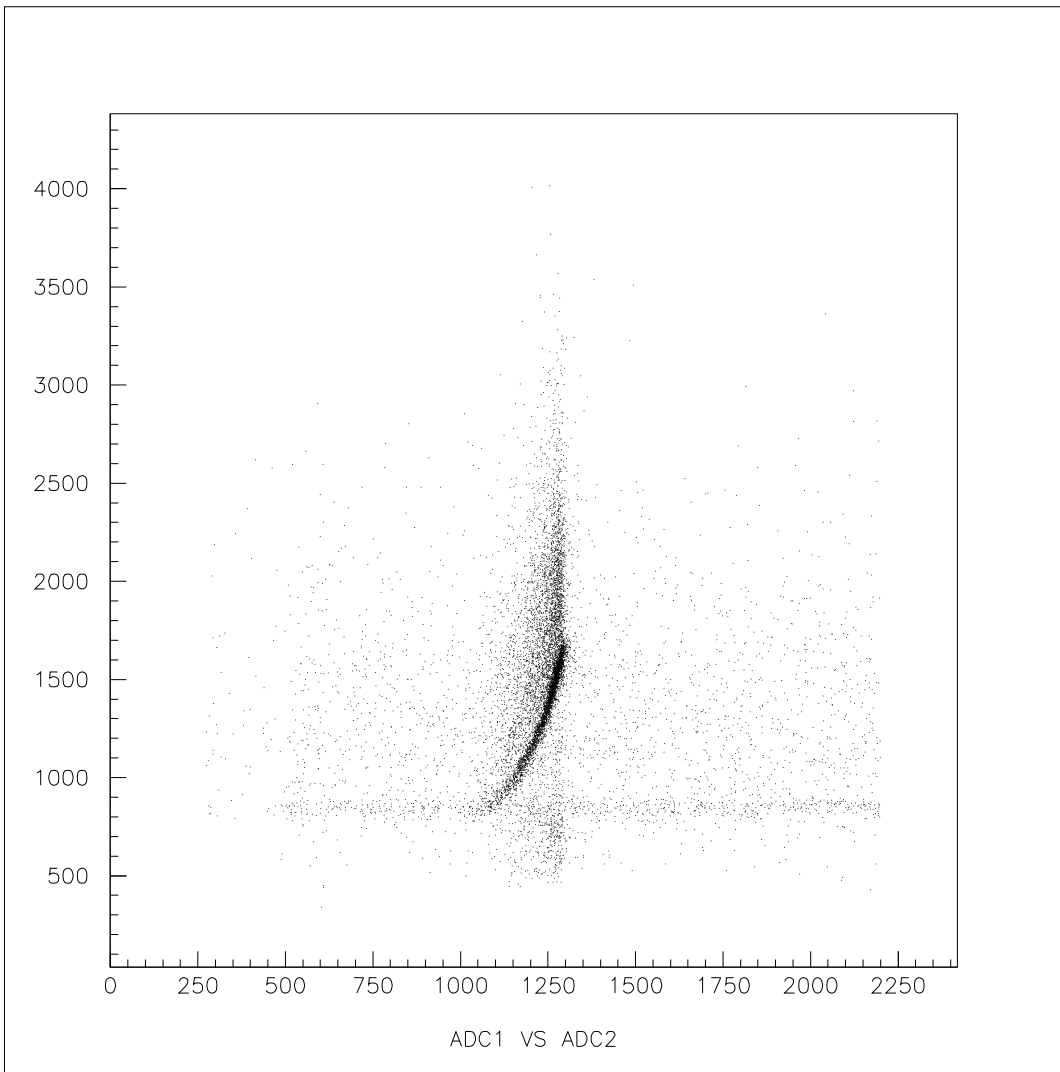


Figure 4

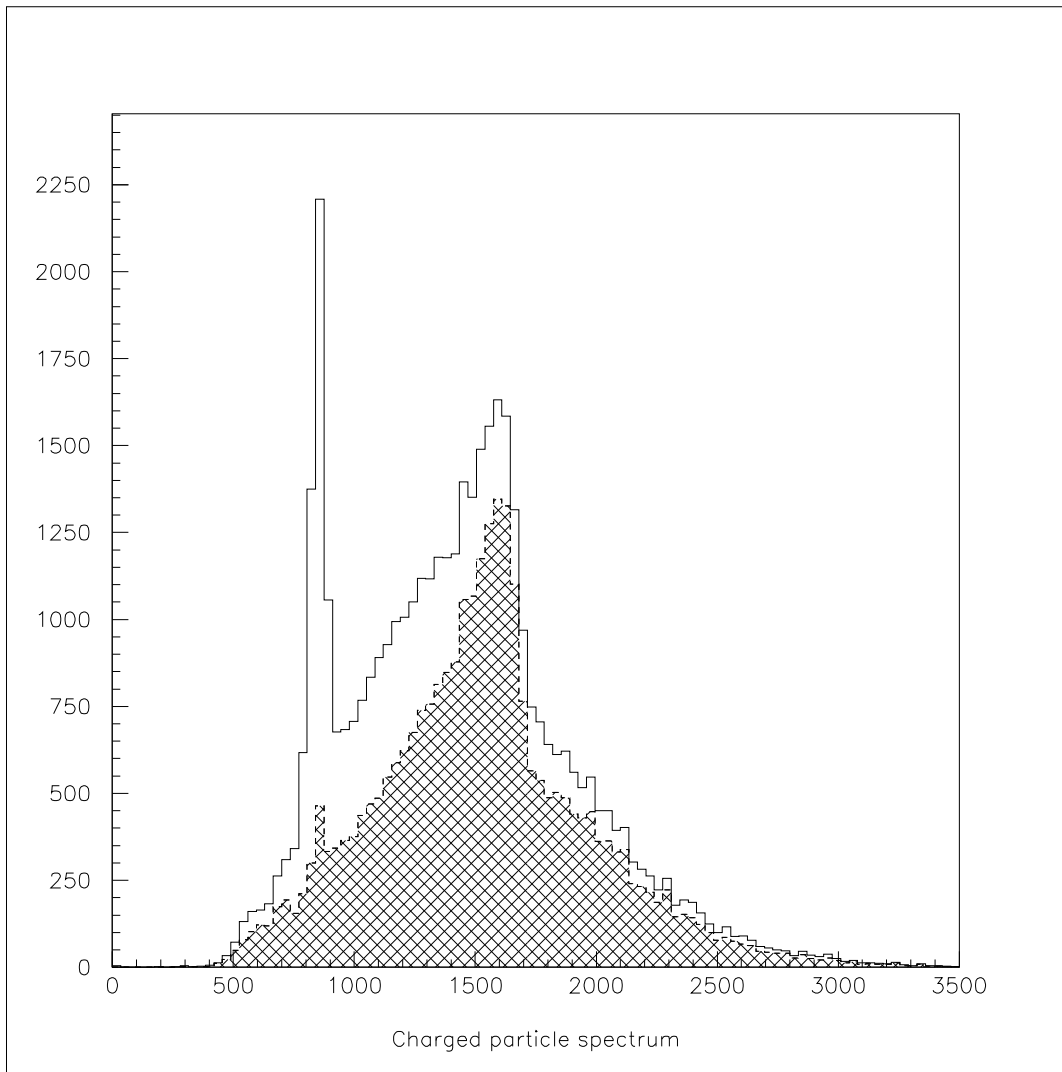


Figure 5

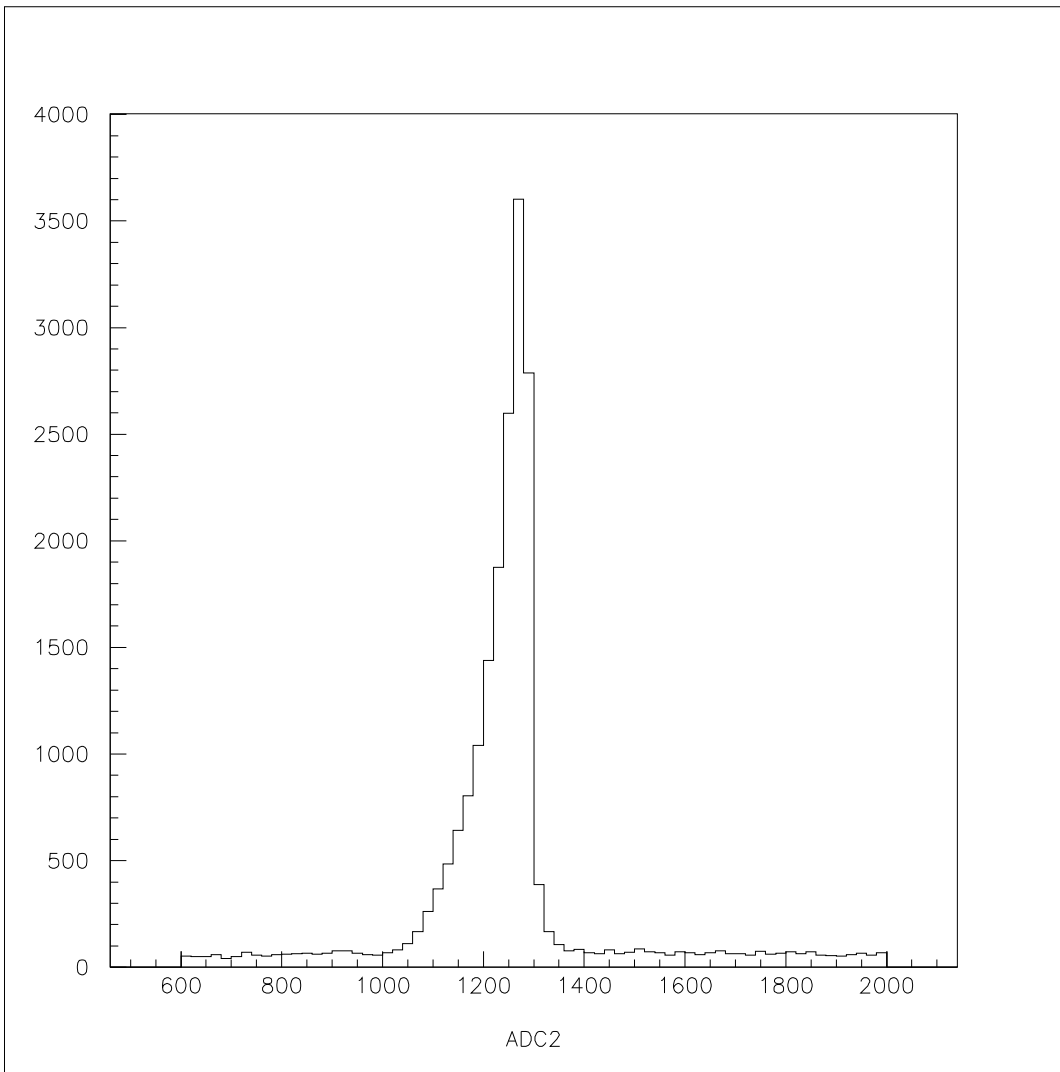


Figure 6

Figure 7

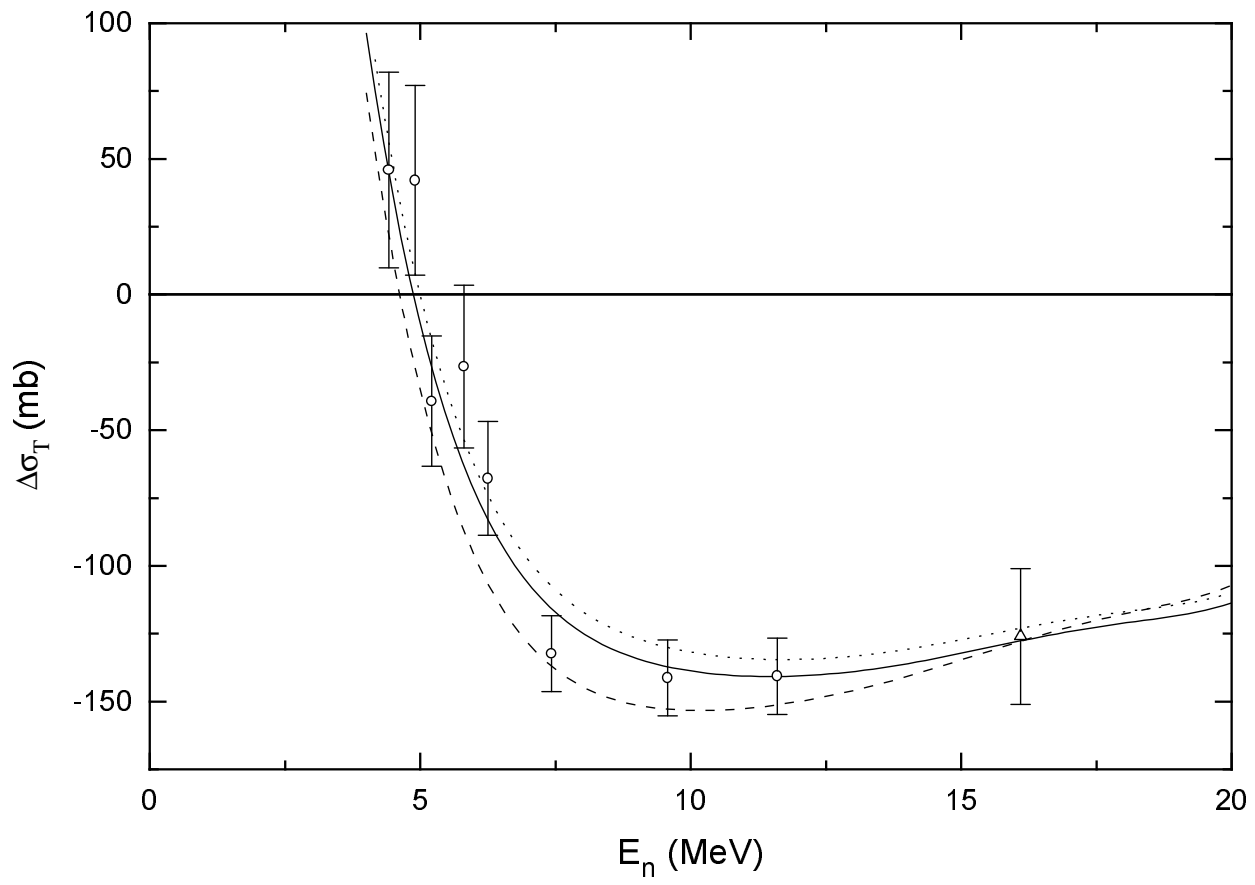


Figure 8

